Experimental evidence for the acceleration of slag hydration in blended cements by the addition of CaCl2

Laurent Steger, Simon Blotevogel, Laurent Frouin, Cédric Patapy, Martin Cyr

Experimental evidence for the acceleration of slag hydration in blended cements by the addition of $CaCl_2$

Laurent STEGER[1,2], Simon BLOTEVOGEL[1], Laurent FROUIN[2], Cédric PATAPY[1*], Martin CYR[1]

1. Université de Toulouse, UPS, INSA, LMDC (Laboratoire Matériaux et Durabilité des Constructions de Toulouse), 135 Avenue de Rangueil, 31077, Toulouse cedex 04, France.
2. Ecocem Materials, 4 Place Louis Armand, 75012 Paris, France.

* Corresponding author

Abstract

Cements with high substitution rates of ground granulated blast furnace slags (GGBS) have the potential to significantly lower CO_2 emissions of concrete, but their early age strength is often below those of traditional OPC cements. One way of mitigating this drawback is to use accelerating admixtures. In this study, the effect of $CaCl_2$ additions on the hydration of blended cements was investigated by measuring compressive strength, porosity, heat release and propagation of ultrasound in blends containing 70 wt.% of GGBS. The onset of formation of aluminate phases was monitored using in-situ XRD. The effect of $CaCl_2$ on slag hydration was isolated by replacing GGBS by an inert quartz filler. Results showed that compressive strength values at one, two and seven days were increased by 50% by the $CaCl_2$ addition. The increases in compressive strength corresponded to a reduction in pore space. GGBS hydration contributed to the heat development, structuration and compressive strength of the blended cements from 15 hours. The addition of $CaCl_2$ led to an earlier onset of the GGBS reaction, at around 10 hours, and increased the rate of GGBS hydration during the first seven days. The time of onset of the GGBS contribution was also the moment when AFm precipitation started. In $CaCl_2$-containing blends, Cl was incorporated in AFm.

Keywords

GGBS, Accelerator, Chloride, Reactivity, Early age

This manuscript was published in Cement and Concrete Research under DOI: 10.1016/j.cemconres.2021.106558

1. Introduction

Due to the high environmental impact of the cement production, current designs of cements aim to reduce their carbon footprint. This is partially achieved by using supplementary cementitious materials (SCM) as clinker substitutes. Ground Granulated Blast Furnace Slag (GGBS), a glassy by-product of pig iron production, is a common SCM that has been used for over 100 years [1], [2]. Partly replacing clinker by GGBS lowers costs and the CO_2 footprint of the material and also enhances its physical and chemical resistance [1], [3]–[5].

Even though large differences exist between different slags, at high substitution levels, GGBS blended cements typically show lower reactivity and early age performance than blends containing higher amounts of clinker [6]–[9]. Some authors have even reported that GGBS does not react during the first 24 hours of hydration, whereas others report a degree of slag reaction between 10 and 30 % after one day of hydration [10]–[16]. The addition of GGBS also influences the clinker hydration. At high clinker replacement levels, the effect of cement dilution becomes greater than the positive filler-effect of increased nucleation sites [17]–[19].

One promising way to compensate for the slower reaction of GGBS is to add accelerating salts such as $CaCl_2$ [7], [20]–[22]. $CaCl_2$ has been known to accelerate the hydration of Portland cement for many years [23]. Even though the exact mechanism of action is still under discussion, recent studies show that the effect of $CaCl_2$ can well be modeled by an increase in the number of nucleii [24]–[28]. Besides, Cl and Ca ions to flocculate hydrophilic colloids and stronger flocculation of C-S-H leads to bigger pores in the C-S-H gel resulting in later diffusion control of the hydration reaction [26]. Furthermore, the presence of Ca increases the supersaturation of the pore solution with Ca bearing mineral phases, including C-S-H.

For GGBS blended cements, Bellmann et al. [7] reported that 2-day strength of GGBS – $Ca(OH)_2$ – cement blends could be increased by a factor of 3 when 3 wt.% $CaCl_2$ was added and Van Rompaey [22] showed an accelerated hydration of GGBS blended cements in the presence of $CaCl_2$. In both studies, it remains unclear whether the increase in short-term performance stems only from an accelerated cement hydration or if the addition of $CaCl_2$ also has a significant impact on the GGBS hydration rate. Also, for fly-ash blended cements,

higher early age compressive strengths have been reported [29]–[31] and studies on natural pozzolanic material have shown that $CaCl_2$ enhances their reactivity [32], [33]. The main disadvantage of the use of $CaCl_2$ is the potentially increased corrosion of steel in reinforced concrete by the presence of Cl ions [34]. But this effect appears to be low in slag blended cements accelerated by CaCl2, because of chloride binding in Al-bearing hydrates [35], [36].

The aim of this work was to investigate if and to what extent $CaCl_2$ accelerates the hydration of GGBS in blends of 70 % GGBS, 30 % cement. In order to identify the effect of $CaCl_2$ on the GGBS hydration, samples of blended cements and model samples where GGBS was replaced by an inert quartz filler were prepared with and without the addition of $CaCl_2$ for different curing times [11]. For all samples, compressive strength development, early age structuration, and heat development during hydration were analyzed. In addition, aluminate formation and pore space evolution were monitored in slag-containing blends.

2. Materials and methods

2.1 Raw materials

An industrial GGBS from ECOCEM Dublin and a CEM I 52.5R (Blaine finenesses of 4350 cm²/g and 4150 cm²/g, respectively), were used for this study. Their chemical compositions are given in Table 1.**Erreur ! Source du renvoi introuvable.** The basicity index CaO/SiO_2 of the GGBS was 1.16 and its amorphous content was > 99% as determined by QXRD.

To simulate the physical impacts of GGBS grains on nucleation, a fine quartz filler (C400 from Sibelco) was selected with a particle size distribution is comparable to that of the GGBS (Figure 1). The SiO_2 content of the quartz, measured by XRF, was >98.5 wt.%. Lab grade $CaCl_2.2H_2O$ from Sigma-Aldrich was used as the accelerating salt. Weight percentages refer to this hydrated $CaCl_2$ form. Sample IDs, compositions and analyses performed on each sample are shown in Table 2. The amount of 1 wt.% $CaCl_2$ was fixed to be high enough to have an observable effect, but below 0.65 wt.% of Cl in the binder pastes, which corresponds to the maximum content allowed in concretes using CEM III cements after EN-206/CN.

Table 1 - Chemical composition, loss on ignition and Blaine surfaces of the raw materials, measured by XRF (GGBS) and ICP-OES (OPC)

		GGBS	OPC (CEM I 52.5R)
SiO_2	wt.%	35.7	20.1
Al_2O_3	wt.%	11.5	4.4
CaO	wt.%	41.5	65.7
Fe_2O_3	wt.%	0.6	2.2
MgO	wt.%	7.6	0.8
K_2O	wt.%	0.4	0.2
Na_2O	wt.%	0.3	0.2
SO_3	wt.%	0.7	3.6
TiO_2	wt.%	0.6	0.2
Cr_2O_3	wt.%	<0.05	<0.05
Mn_2O_3	wt.%	0.4	0.1
P_2O_5	wt.%	<0.05	0.1
F	wt.%	<0.04	0.1
L.O.I (%)	wt.%	0.8	2.5
Blaine	cm^2/g	4350	4150

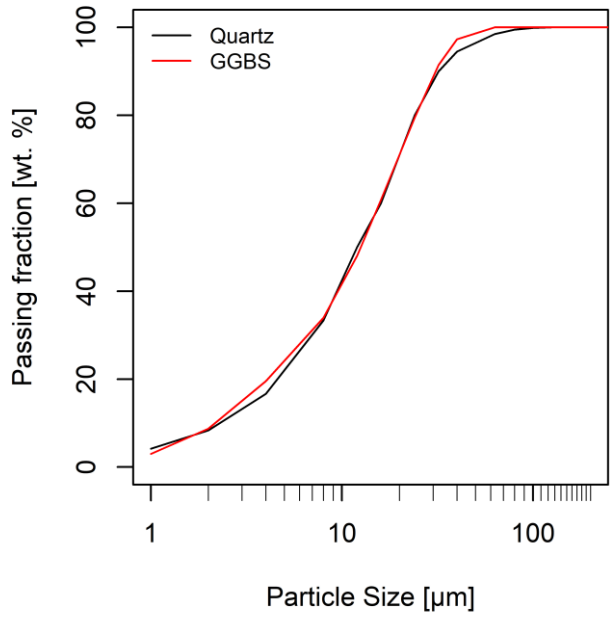

Figure 1. Particle size distribution of the quartz filler and the GGBS, measured by laser diffraction granulometry in an ethanol suspension.

2.2 Compressive strength

Test prisms (40 mm × 40 mm × 160 mm) were cast from mortars containing one part of binder and three parts of normalized sand, according to the standard EN 196-1:2016. The water/binder (W/B) ratio was 0.5 and mixtures were prepared using standardized CONTROLS Automix 65 mixers. If $CaCl_2$ was used for a sample, it was dissolved in the mixing water prior to mixing. After demolding at 24 hours, the mortar prisms were cured under water at 20°C until the different curing ages were reached. The mechanical strengths were determined by compression tests. The 7- and 28-day samples were tested using a standardized press from 3R. The samples aged 1 and 2 days were tested on a standardized press by IGM, with controlled loading and a speed of load application reduced to 1200 N / s (2400 N / s in EN 196-1:2016).

2.3 Ultrasound propagation velocity

The ultrasound propagation velocity (Vp) measurements were carried out on an Ultra Test IP-8 instrument on binder pastes with a 0.4 W/B ratio. The samples were prepared on the basis of 100 g of dry binder and 40 g of water. The accelerator was dissolved in water. When an accelerator was incorporated, the solution was left to stand for 10 minutes in order to dissipate the heat generated by $CaCl_2$ dissolution. The solution was then poured onto the powder and the whole was mixed with an electric mixer set at a rotation speed of 1500 rpm for 2 minutes. The Vp evolution was monitored for 3 days at the rate of one measurement every 2 minutes.

2.4 Isothermal calorimetry

Calorimetric tests were carried out using a TAM Air isothermal calorimeter from TA-instruments, set at 20 °C. Samples were prepared as described in section 2.3. Measurements were carried out on 10 g samples of pastes in a sealed measurement vessel. Heat development was measured for 72 hours, with a step of 50 seconds between consecutive measurements. The sample preparation (mixing + ampoule filling) was performed outside the calorimeter. This method destabilized the temperature of the chamber during the introduction of the sample and invalidated the first few minutes of measurements, therefore the measurements were started at 45 min of reaction. However, the "internal" mixing

methods did not make it possible to obtain a homogeneous mixture in the case of viscous binders such as cement pastes and thus might have led to unrepresentative results [37].

2.5 SEM observations

A semi-quantitative evaluation of the porosity of the slag-containing binder pastes was made by scanning electron microscope (SEM) image processing [11], [38]. A series of 30 images per sample were taken in back-scattered electron mode (x5000) on a JEOL JSM7100F, operated at 15 keV. These machine settings theoretically allow to resolve features down to 18.8 nm, actual object size may be somewhat higher. At this resolution air voids and capillary pores are well resolved, but gel pores are not [39]. The thresholding was carried out using a k-means algorithm. The grey level histograms of each SEM image were thereby segmented into 6 classes. The first group, with the lowest grey level, was defined as porosity. To be able to compare different SEM images, the grey level histograms were adjusted to represent the same minimum and maximum grey levels. Elemental analysis was carried out using an SDD x-max detector from Oxford Instruments.

Cement paste samples were prepared in cylindrical 60 mL poly-propylene recipients. Same as for mortar samples, the paste samples were demolded at 24h and, if applicable, further cured under water. For SEM analysis a slice of the paste sample was cut by a circular saw and hydration was stopped at 1 day, 2 days and 7 days by immersing the slice overnight in isopropanol. A fracture of the center of the cut slice was then vacuum-impregnated into an epoxy resin. Sample surfaces were polished for 4h using an argon ion beam cross section polisher (IB-19510CP, by JEOL) operating at 6kV. Samples were not mechanical prepolished due to their instability.

2.6 In situ XRD (IS-XRD) of early hydration

Fresh slag-containing binder pastes (S70 and S70Cl1) were encapsulated between two Kapton foils (7.6 µm thickness, by LGC) and scanned every 45 min for the first 31.5 hours of hydration. Sample weight remained constant before and after analysis, suggesting not evaporative loss of hydration water. The measurements were carried out on a Bruker D8 Advance diffractometer under Cu-Kα radiation in a Bragg-Bretano configuration. The scans

were operated between 8 and 70° 2θ with a 0.02° step and a scan time of 0.31 s per step for a total scan time of around 20 minutes.

Table 2. Overview of sample composition and analysis performed on each sample

ID	Sample Composition				Analysis				
	Slag	Quartz	Cement	$CaCl_2$	Sc	US	Cal	IS-XRD	SEM
	wt.%	wt.%	wt.%	wt.%	-	-	-	-	-
S70	70	0	30	0	x	x	x	x	x
S70Cl1	70	0	30	1	x	x	x	x	x
Q70	0	70	30	0	x	x	x	-	-
Q70Cl1	0	70	30	1	x	x	x	-	-

Amounts of slag, quartz and cement refer to the powder composition. $CaCl_2$ refers to the amount of $CaCl_2.2H_2O$ with respect to the sample powder dissolved in the mixing water. Abbreviations for analysis are: Sc – Compressive strength tests, US – ultrasound propagation measurements, Cal – isothermal calorimetry, IS-XRD – in situ X-ray diffraction measurements, SEM – porosity analysis by scanning electron microscope image processing.

3. Results

3.1 Compressive strength

The compressive strengths of mortars containing 70% slag (S70) and 70% quartz (Q70), with and without addition of 1 wt.% $CaCl_2$, are presented in Figure 2. In the pastes containing slag and cement (S70), the addition of $CaCl_2$ increased 1-day compressive strength from 3.83 ± 0.14 to 5.65 ± 0.16 MPa, 2-day compressive strength from 8.52 ± 0.45 to 11.99 ± 0.62 MPa and 7-day compressive strength from 25.83 ± 0.40 to 37.48 ± 0.60 MPa. This represents a relative increase of compressive strength of almost 50% due to the $CaCl_2$ addition. After 28 days of hydration, only a slight difference in compressive strength remained between the two mixtures.

In the pastes containing quartz filler and cement (Q70), compressive strength was below that of slag and cement at all curing times (Figure 2). Compressive strength increased only slowly from 3.33 ± 0.02 MPa at 1 day to reach 9.67 ± 0.16 MPa after 7 days. The addition of $CaCl_2$ had only a slight positive effect on compressive strength development after 1 day of curing (3.69 ± 0.07 MPa). At 2 days of hydration, there was no significant difference between the two treatments and, at 7 days, the compressive strength of the sample with $CaCl_2$ addition was below that of the sample without addition.

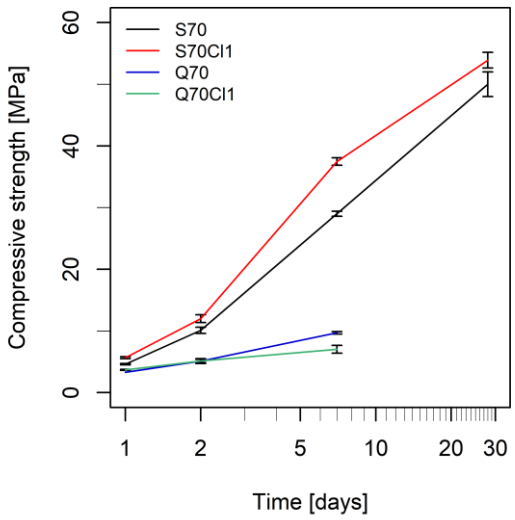

Figure 2. Compressive strength of blended cements with 70 wt.% of GGBS with (S70-Cl1) and without (S70) $CaCl_2$ addition, 70 wt.% of inert quartz filler with (Q70-Cl1) and without (Q70) $CaCl_2$ addition. Values are given for systems with and without 1 wt.% $CaCl_2$ addition. Note that the time is represented on a logarithmic scale.

3.2 Heat of hydration

Heat flow curves of $CaCl_2$ accelerated samples (S70Cl and Q70Cl) showed a main peak of about 2 mW/g at around 4 hours of hydration (Figure 3). In samples without $CaCl_2$ addition, the main heat flow peak appeared at around 10 hours, with a heat flow of about 1.5 mW/g. This main peak was probably due to cement hydration, as the shape and amplitude were similar between slag- and quartz-containing samples. Consequently, the observed effect of $CaCl_2$ addition on the main hydration peak shows its effect on cement.

At later stages of hydration, the slag-containing systems showed higher heat flow values than the quartz-containing systems. This effect was visible in the $CaCl_2$ accelerated systems from about 10 hours onward and on the systems without accelerator addition from 15 hours. Heat flows of the slag-containing systems started to converge from 15 hours onward, until heat flow became higher in S70 than S70Cl1 from 52 hours on. In quartz-containing systems Q70 and Q70Cl1, heat flow was almost identical starting from 15 hours.

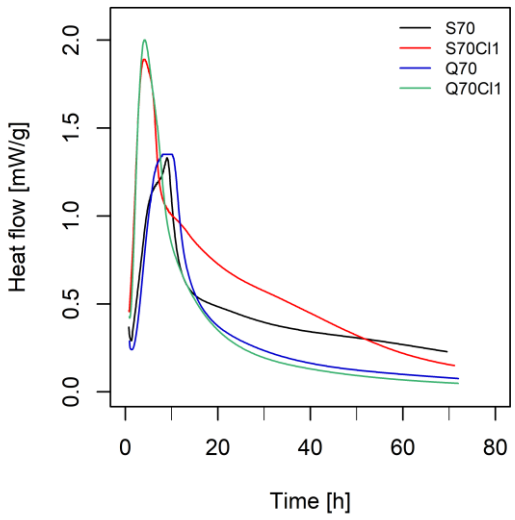

Figure 3. Heat flow in blended cements with 70 wt.% of GGBS (S70) and 70 wt.% of inert quartz filler with the same PSD (Q70). Values are given for systems with and without 1 wt.% $CaCl_2$ addition.

Cumulative heat results are shown in **Erreur ! Source du renvoi introuvable.**4a. After around 2 hours, the two pastes containing $CaCl_2$ started to show an increase in heat release, the time of occurrence and intensity of which are comparable. For the samples without $CaCl_2$, heat development started at about 4 hours (Figure 4a). The accelerating effect of $CaCl_2$ at this point in time probably came from its action on the cement. Subsequently, an additional contribution to the heat release was observed from around 15 hours onward for the slag-containing samples and from 10 hours for slag-containing samples with CaCl2 addition (S70 and S70Cl1). This increase in reaction heat was probably due to the start of the slag hydration.

In Q70 and Q70Cl1 samples, the heat development rate decreased after 15 hours and the two samples started to converge (Figure 4a). This observation indicates a lower contribution of $CaCl_2$ additions to the heat development at later stages of the experiment.

3.3 Ultrasound propagation during hydration

The speed of sound in cement pastes containing 70% slag (S70) and 70% quartz (Q70), with and without addition of 1 wt.% $CaCl_2$, is presented in Figure 4b. The variation of the speed of sound in cement pastes is usually divided into three stages: 1. Dormant phase, controlled by

the speed of sound in air bubbles that were introduced during mixing, 2. Rapid increase to about 1500 m/s when the speed of sound becomes controlled by water, and 3. A progressive increase due to the formation of hydrates [40]–[43]. All samples showed the typical increase from the speed of sound in air (340 m/s), up to the speed of sound in water (1500 m/s) within the first hours of hydration (Figure 4b).

This first characteristic increase in the speed of sound occurred earlier in S70Cl1 (around 2.5 hours) than in S70 (around 5 hours). From this first characteristic step onwards, the speed of sound increased steadily in both samples and remained higher in S70Cl1 than in S70 during the whole experiment (Figure 4b). After about 30 hours of hydration, the difference between S70Cl1 and S70 started to increase further.

Similarly, in the pastes containing quartz and cement (Q70) the initial increase of speed of sound occurred slightly earlier for pastes containing $CaCl_2$ (Figure 4b). After the first characteristic step, the speed of sound increased further, but only slowly. Starting from 12 hours, the speed of sound in both samples containing slag was higher than in the sample containing quartz with $CaCl_2$ addition. After approximately 36 hours, the speed of sound became higher in the $CaCl_2$-free sample.

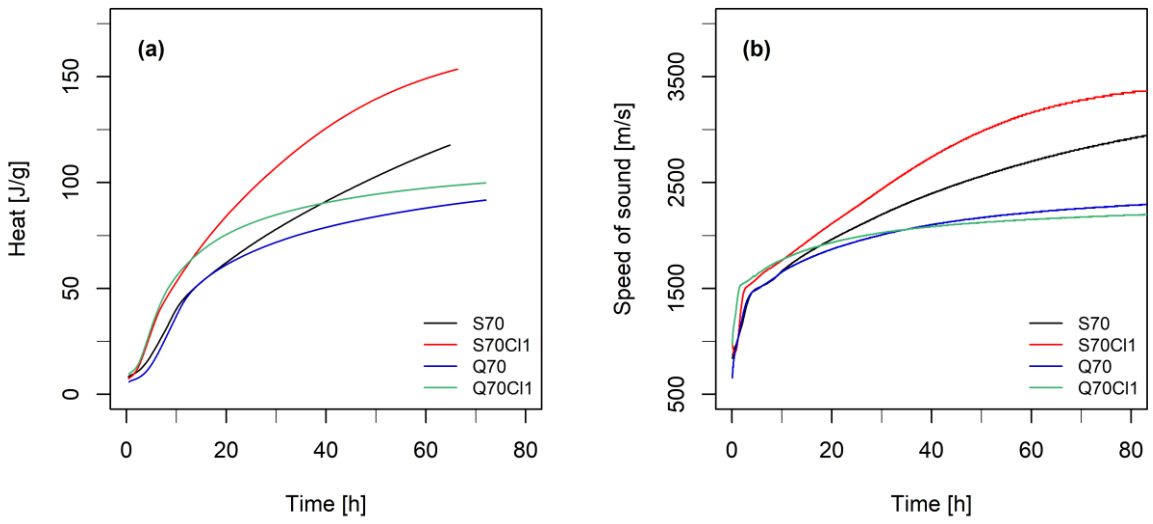

Figure 4. (a) Cumulative heat (per gram of binder) of cement paste samples containing 70% slag (S70) and 70% quartz (Q70), with and without addition of 1 wt.% $CaCl_2$ (S70Cl1 and Q70Cl1). (b) Speed of sound during the hydration reaction of the same samples

3.4 In-situ XRD analysis

XRD patterns of the last in-situ scan, after 31.5 hours of hydration of S70 and S70Cl1, are shown in Figure 5. Both patterns show multiple amorphous humps corresponding to the presence of slag, water, the Kapton film and probably amorphous hydrate phases during in-situ analysis. In addition, both samples show Bragg peaks corresponding to the anhydrous cement phases C_3S and C_2S with similar intensities.

Furthermore, both XRD patterns show characteristic peaks of typical hydrate phases, portlandite and ettringite, in similar intensities. One obvious difference between the samples is the higher intensity of the first AFm peak in S70Cl1 compared to S70. There is also a difference in the position of the first AFm peak, which appears at 10.7° for S70 and at 10.9° for S70Cl1. In addition, a second AFm peak also appears earlier in S70 (21.7°) than in S70Cl1 (22.0°). For both samples, the position of the second peak corresponds to the double d-spacing of the first peak. The third AFm peak is, however, at the same position for S70 and S70Cl1, suggesting only unidimensional differences in crystal structure between the two samples, which could be induced by a different interlayer anion.

To give a closer look at aluminate formation in S70 and S70Cl1, Figure 6 presents the evolution of intensities over time for an angular range between 8.5° and 11.5°. Ettringite formation was observed in both samples with a discernable peak at about 9.1° 2θ from about five hours on in the S70 sample (Figure 6a) and from 1.5 hours on in the S70Cl1 sample, with $CaCl_2$ addition (Figure 6b).

In the S70 sample, a discernable AFm peak appeared after about 15 hours of hydration. The peak was centered between 10.6° and 10.7° 2θ , which is typical for AFm solid solutions of various anions or hemicarboaluminate [37]. In the S70Cl1 sample the AFm peak appeared from 10 hours and was centered between 10.9° (8.1 Å) and 11.0° 2θ (8.0 Å), indicating smaller d-spacing than in S70. The peak was at slightly higher angles than indicated for AFm solid solutions of OH, SO_4 and CO_3, but below angles typical for Friedel's salt or monosulphate [37]. When hydration was stopped after 24h the AFm peak shifted towards slightly higher angles (around 11.2 ° 2θ (7.89 Å)), in line with the presence of Friedel's salt (data not shown). The AFm peak in S70 split into two large peaks one at lower angle (around

10.4 ° 2θ (8.50 Å)), still in the range of AFm solid solutions and one at higher angles (around 11.7 ° 2θ (7.56 Å)) in line with the presence of monocarboaluminate [37].

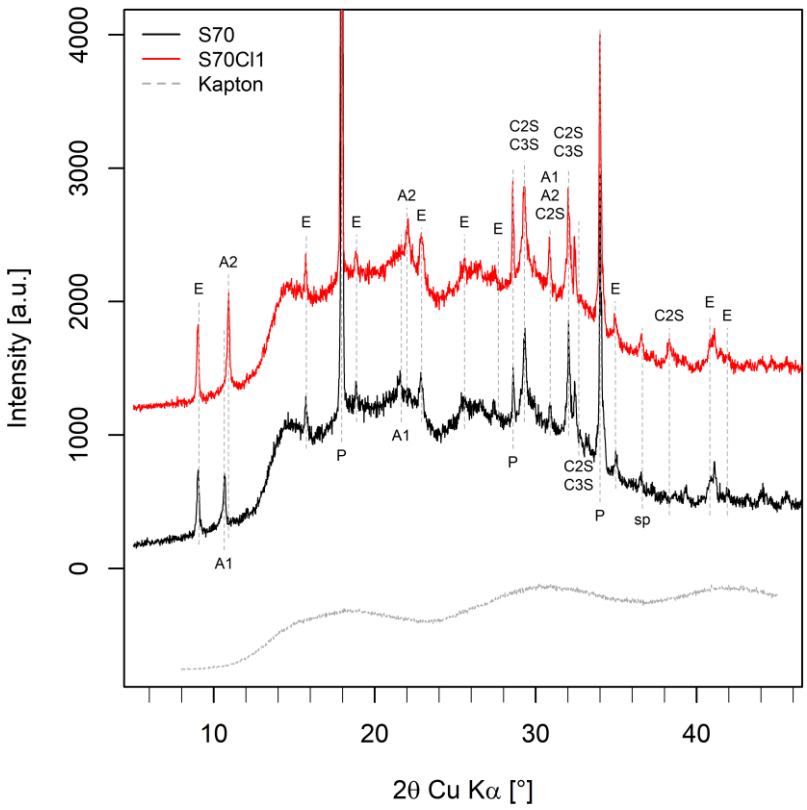

Figure 5. In situ XRD pattern of S70 and S70Cl1 after 31.5 hours of hydration. The diffraction pattern of S70Cl1 was shifted by +1000. Peaks were identified using d-spacings from [37]. Peaks correspond to (E) Ettringite; (A1) AFm-1; (A2) AFm-2; (P) Portlandite; (C2S) Dicalciumsilicate; (C3S) Tricalciumsilicate; (sp) Spinel. The grey, dashed line indicates the diffraction pattern of the Kapton tape, note that intensities are only approximate as the detector has been replaced between sample and Kapton blanc measurements.

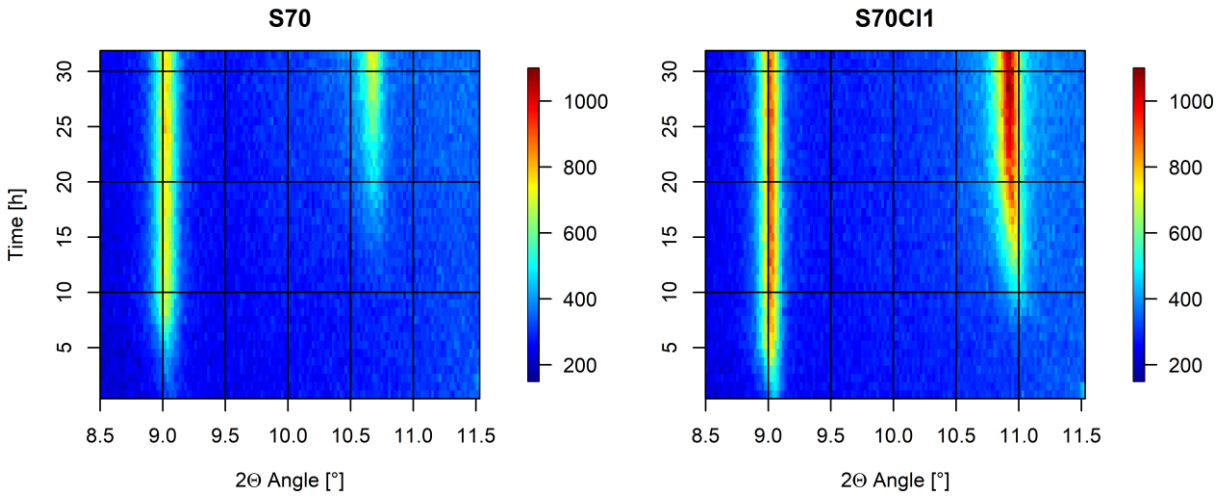

Figure 6. XRD scans between 8.5° and 11.5° 2ϑ of (A) S70 and (B) S70Cl1 during the first 31.5 hours of hydration. Scans were performed every 45 min. The color scale represents the signal intensity in number of counts.

3.5 SEM observations

Figure 7 shows backscattered electron images of S70 and S70Cl1 at x5000 fold magnification after 1 day of hydration, together with the corresponding element maps from EDX analysis. In both samples, a significant amount of hydrates containing Si and Al is visible around slag grains. In S70Cl1, however, there are clear mineral structures visible in pore spaces with high Al intensity. Cl was detected in the same spaces, indicating that it was incorporated into AFm phases.

The evolution of porosity obtained from image processing of S70 and S70Cl1 samples is represented in Figure 8a. Initially porosity of the powdered samples was around 55 vol.%. The porosity decreased during the hydration of both samples. In the S70 samples, porosity was 33 vol.% after 1 day, 28 vol.% after 2 days and 17 vol.% after 7 days of hydration. Decline in porosity was quicker in the S70Cl1 sample with a porosity of 25, 19 and 16 vol. % after 1, 2 and 7 days, respectively. After 7 days of hydration, there was no longer any significant difference between the samples.

Figure 8b shows the relationship between compressive strength and porosity. Compressive strength appears to increase exponentially with decrease in porosity, independently of the sample type.

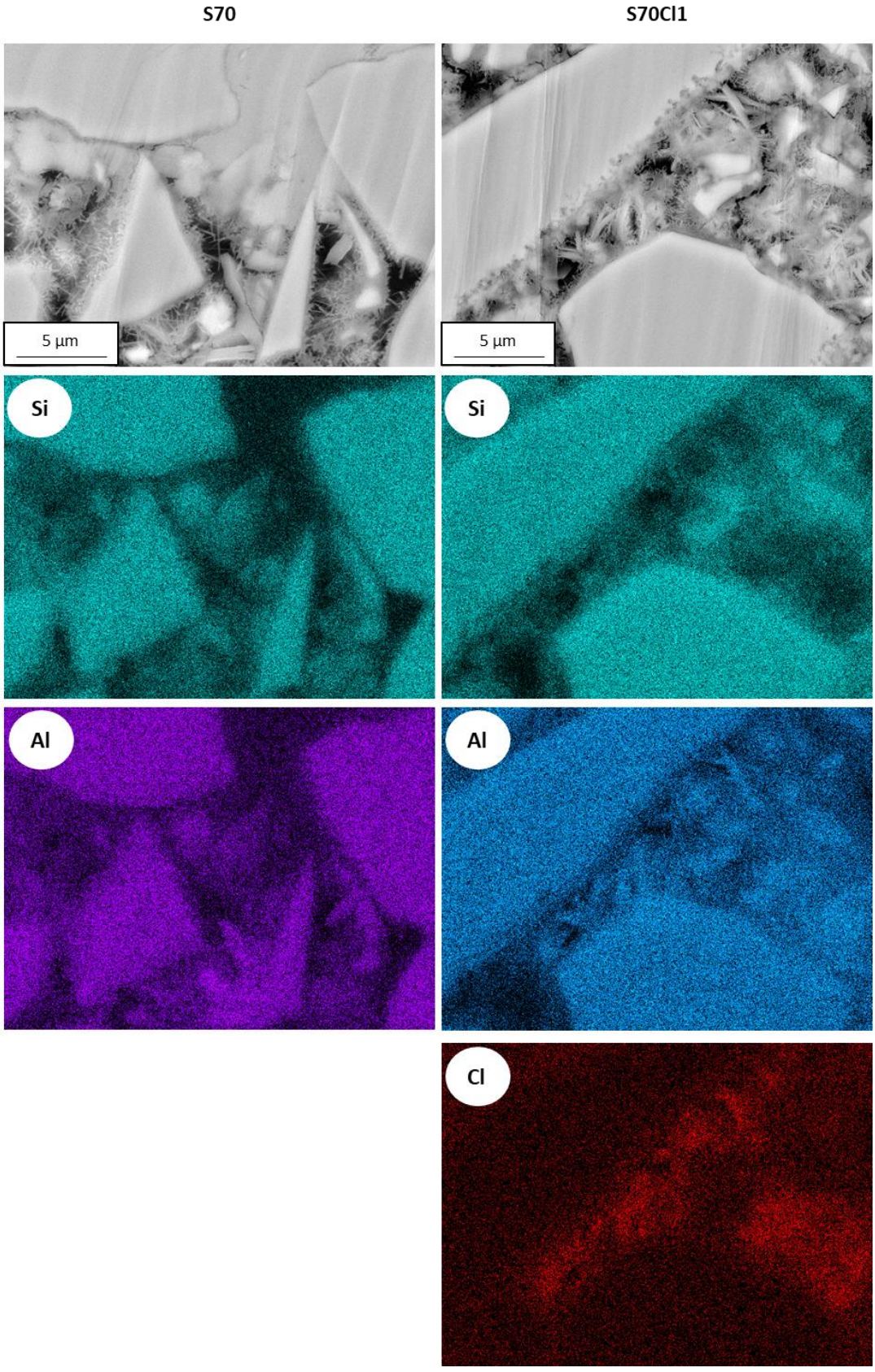

Figure 7. SEM image at x5000 magnification in back-scattered electron mode after 1 day of hydration, and EDX maps of Si, Al and Cl - for S70 on the left and S70Cl1 on the right.

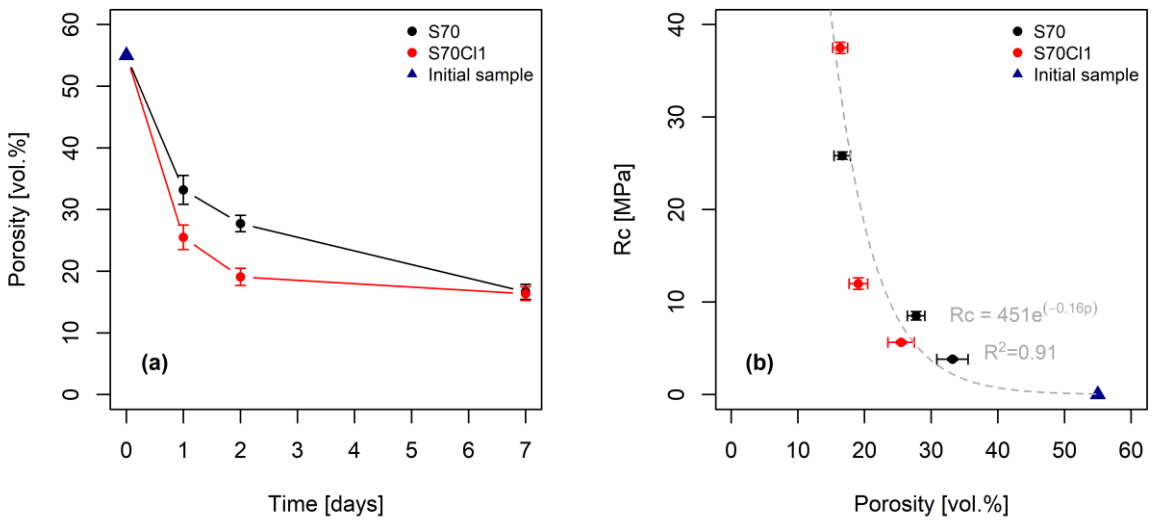

Figure 8. Porosity of S70 and S70Cl1 samples derived from SEM image analysis. (a) Development of porosity over time. (b) Relationship between porosity and mortar compressive strength. The grey dashed line corresponds to the power law $Rc = 451e^{(-0.16p)}$.

4. Discussion

4.1 Contribution of slag to the compressive strength

After a curing time of 1 day, the compressive strength in S70 samples was slightly but significantly higher than in Q70 samples (Figure 2). Since the quartz addition had the same reactive surface area as the slag, this effect cannot be attributed to a physical effect of nucleation but indicates a probable contribution of the GGBS hydration to compressive strength already at 1 day. Calorimetric measurements support this finding by showing an increase in heat development in slag-containing blends (S70 and S70Cl1) after about 15 hours and 10 hours of reaction, which was not detected in blends containing quartz (Figure 4a). This observation is in line with other studies reporting significant degrees of slag hydration at 1 day of hydration [11]–[14], [16]. In contrast, a study on 40 wt.% GGBS blended cements reported a significant contribution of GGBS only after 30 hours [15].

The increase in compressive strength between 1 and 2 days of curing and between 2 and 7 days was also larger in S70 samples (4.7±0.5 and 17.3±0.6 MPa, respectively), than in Q70 samples (1.7±0.4 and 4.6±0.4 MPa, respectively). The observations also correspond well to calorimetric and speed of sound measurements, which show increasing differences between

S70 and Q70 samples from about 10 hours (Figure 4). This shows that the slag hydration makes a significant contribution at these curing ages.

4.2 Effect of $CaCl_2$ addition on slag-containing blends

Significant differences in compressive strength between the S70Cl1 and S70 samples for curing ages of 1, 2 and 7 days illustrate that the addition of $CaCl_2$ accelerates the hydration reaction of blended cements [7], [22]. The higher compressive strength in S70Cl1 compared to S70 is associated with a faster decrease in porosity in the $CaCl_2$-containing blend (Figure 8). S70 and S70Cl1 samples show the same dependence between porosity and compressive strength, suggesting that the pore filling rate and thus the volume of hydrates formed exerts the major control on the compressive strength in both systems. The higher pore filling rate might be attributable to the increased number of nuclei induced by the chloride ion and the supplementary Ca in solution [24]–[28]. This accelerating effect is well documented for cement and its constituents, but the question of whether the slag hydration is also accelerated by the addition of $CaCl_2$ was not yet addressed [24], [26], [44]–[46]. Possible mechanisms for the acceleration of slag hydration will be discussed in section 4.3.

The addition of $CaCl_2$ also had an effect on the formation of aluminate phases (Figure 5). S70Cl1 showed earlier onset of ettringite and AFm formation. Furthermore, S70Cl1 produced AFms with smaller interlayer spacings, close to those expected for Friedel's salt. This suggests the incorporation of Cl as the major interlayer anion if the sample was accelerated by $CaCl_2$. AFm are layered double hydroxydes, in which the interlayer anion can be easily exchanged and the main difference between Friedel's salt and other AFm phases is only the nature of the interlayer anion, which determines the size of the interlayer space. The exchange does not need to be complete so that AFms exist in solid solutions with various interlayer anions, this implies that the peak positions in cement samples are not necessarily the same as for pure phases [37], [47]. SEM observations supports the incorporation of Cl into AFm phases, even though SEM analysis cannot distinguish between surface adsorption and incorporation of Cl. The incorporation of Cl into AFm phases might lead to an earlier oversaturation with AFm compared to systems without $CaCl_2$ addition. However, In earlier studies, the formation of Cl containing phases was associated with the removal of Cl from solution and subsequent decrease in hydration rates [44]–[46]. Binding of Cl into Al bearing

hydrates was already reported in slag cements and potentially reduces the corrosion risk in reinforced concrete [35], [36].

The appearance of AFm in the in situ XRD patterns (Figure 6) coincides with the start of higher heat release of slag-containing blends (10 hours for S70Cl1 and 15 hours for S70) with respect to quartz-containing blends (Figure 4). This suggests that slag hydration and AFm formation are linked.

4.3 The GGBS reaction in the presence of $CaCl_2$

To be able to distinguish between cement hydration, slag hydration and physical effects, blends containing 70% of quartz as an inert filler (Q70) were prepared. To further investigate the effect of $CaCl_2$ addition on the GGBS hydration, the effect of the GGBS on heat release and speed of sound propagation was computed as the difference between S70 and Q70 systems (Eq. 1) [11]. The difference between the Q70 and S70 systems can be interpreted as the effect of GGBS on the hydration reaction, because the quartz is considered inert and cement is present in the same proportions in the two systems. However, this approach assumes that the reaction of cement is the same in the presence of quartz and slag. This was shown to be not accurate as the degree of reaction of cement was reported to be lower (-8 % in a 40% slag – 60 OPC mix) in the presence of slag than in the presence of quartz [15]. Therefore, results of the subtraction method likely underestimate the contribution of GGBS to the heat replace and the increase in speed of sound. The resulting heat and speed of sound curves are displayed in Figure 9.

$$\Delta Q_i = Q_{(S70)} - Q_{(Q70)} \text{ (J/g cement)} \quad (1)$$

Where ΔQ_i represents the increase of heat release or speed of sound due to the presence of GGBS. The heat release or speed of sound during the hydration of the S70 or S70Cl1 systems is represented by $Q_{(S70)}$ and the heat or speed of sound the corresponding system containing the quartz filler by $Q_{(Q70)}$.

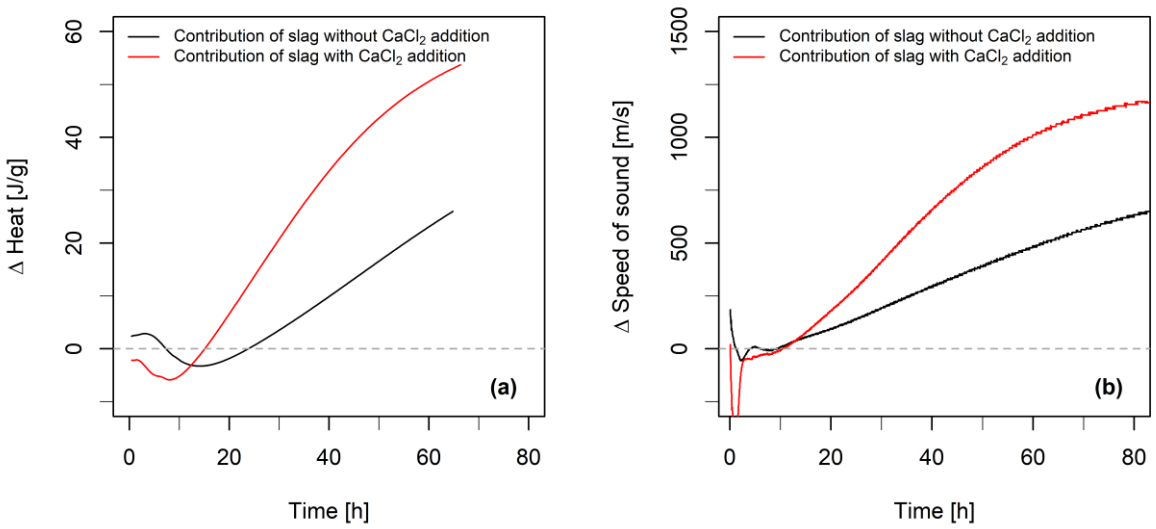

Figure 9. Contribution of GGBS hydration to heat development (a) and speed of sound evolution (b), computed as the difference between S70 and Q70, and S70Cl1 and Q70Cl1 systems.

The contribution of GGBS to heat development during the hydration reaction is around zero at the beginning of the reaction and passes through an initially negative phase (Figure 9a). This negative contribution is probably due to small differences in the filler effect of GGBS and quartz filler and to the fact that the liberation of ions from the GGBS decreases the cement dissolution slightly [15], [16]. For the system without $CaCl_2$ addition, the GGBS contribution to the reaction heat reaches a minimum at around 15 hours and steadily increases from then on. This observation shows that GGBS hydration starts to contribute significant heat from 15 hours in blended cements. This is earlier than formerly reported in the literature but in line with significant slag hydration at 1 day of age [10]–[16]. Note that this point in time corresponds to the onset of AFm formation (Figure 6a). For the accelerated system, the minimum was already reached at about 10 hours (Figure 9a). Again, this was the moment when AFm formation started (Figure 6b).

For this first reaction phase, no differences in speed of sound were observed between the two systems. This may be attributable to the imprecisions of the speed of sound measurements during the early hours of the reaction, when the speed of sound is still controlled by air bubbles from the mixing process, or by the fact that the initial heat release is due to the dissolution and not to hydrate formation.

Between 10 and 36 hours, there was a steeper increase in heat contribution for the accelerated system compared to the system without $CaCl_2$ addition. In speed of sound measurements, a corresponding increase was observed between 10 and 36 hours, suggesting that heat release was actually linked to the formation of stronger solid connections in the sample (Figure 9b). After 40 hours, the heat contribution of GGBS and its contribution to the increase of the speed of sound started to slow down.

These observations show that $CaCl_2$ has an accelerating effect on the GGBS hydration in blended cements. This is in line with, the acceleration of OPC-free, GGBS-based binders by $CaCl_2$ [7], [48]. As for the cement, the GGBS hydration started earlier in the systems containing $CaCl_2$ and its intensity also increased during the first days of hydration. With the present dataset, it is not possible to judge which mechanisms actually accelerated the slag hydration. The mechanisms that were identified for the acceleration of cement phases could also benefit the slag hydration. For instance, the formation of more porous hydrates would also increase the diffusion of ions from the slag surfaces and retard the diffusion control of the hydration reaction [24], [26], [27]. A higher nucleation rate would also benefit GGBS hydration [24]. Besides, a higher polymerization degree of Si was observed in C-S-H from C3S hydration in the presence of $CaCl_2$, implying a stronger connectivity of C-S-H units [49]. This finding can also be applied to C-S-H resulting from GGBS hydration. Besides these two mechanisms described for cement, it has been reported that chloride salts increase the affinity of water for GGBS surfaces, which could enhance the slag dissolution [50].

5. Conclusion

Using multiple macroscopic approaches, it was shown that the hydration of GGBS started to contribute to heat development and increased speed of sound from 15 hours onward in 70% GGBS blended cement pastes. This contribution resulted in significantly higher compressive strength in blended cements containing 70% of GGBS compared to the same cement blended with an equivalent amount of inert quartz filler. The addition of 1 wt.% of $CaCl_2$ led to an earlier onset of heat development. This was observed in blends containing GGBS and the inert quartz filler, so these observations probably have been due to the accelerating effect of $CaCl_2$ on the cement.

After 10 hours of hydration, the addition of $CaCl_2$ increased heat release and the speed of sound much more strongly in GGBS-containing blends than in blends with an inert quartz filler. These observations indicate an increased intensity of GGBS hydration due to the $CaCl_2$ addition. Furthermore, an earlier onset of the slag reaction was observed, at around 10 hours, compared to 15 hours in systems without $CaCl_2$ addition. In both systems, the onset of slag hydration coincided with the onset of AFm formation determined by in-situ XRD.

The enhanced GGBS hydration resulted in significantly higher compressive strength values at 1, 2 and 7 days of hydration, compared to slag blended cements without $CaCl_2$ addition. Increased compressive strength corresponded well to a faster decline in porosity, suggesting that a higher rate of pore filling was responsible for the increase in compressive strength. After 28 days, compressive strength was similar in both the systems - with and without $CaCl_2$ addition.

Acknowledgements

This research project received financial support from ECOCEM Materials. The authors thank Arnaud Proietti and Claudie Josse for help with sample preparation and SEM analysis at the Raymond Castaing Center in Toulouse.

Conflicts of interest

The authors declare no conflict of interest

6. References

[1] W. Matthes *et al.*, « Ground Granulated Blast-Furnace Slag », in *Properties of Fresh and Hardened Concrete Containing Supplementary Cementitious Materials*, Springer, Cham, 2018, p. 1‑53. doi: 10.1007/978-3-319-70606-1_1.

[2] H. F. W. Taylor, *Cement Chemistry*. Thomas Telford, 1997.

[3] B. Lothenbach, K. Scrivener, et R. D. Hooton, « Supplementary cementitious materials », *Cement and Concrete Research*, vol. 41, n° 12, p. 1244‑1256, déc. 2011, doi: 10.1016/j.cemconres.2010.12.001.

[4] P. Van den Heede et N. De Belie, « Environmental impact and life cycle assessment (LCA) of traditional and 'green' concretes: Literature review and theoretical calculations », *Cement and Concrete Composites*, vol. 34, n° 4, p. 431‑442, avr. 2012, doi: 10.1016/j.cemconcomp.2012.01.004.

[5] M. Moranville-Regourd, « 11 - Cements Made From Blastfurnace Slag A2 - Hewlett, Peter C. », in *Lea's Chemistry of Cement and Concrete (Fourth Edition)*, Oxford: Butterworth-Heinemann, 1998, p. 637‑678. Consulté le: sept. 16, 2016. [En ligne]. Disponible sur: http://www.sciencedirect.com/science/article/pii/B9780750662567500230

[6] E. Lang, « Chapter 12. Blastfurnace cements », in *Structure and performance of cements, 2nd edition*, 2002, p. 310‑325.

[7] F. Bellmann et J. Stark, « Activation of blast furnace slag by a new method », *Cement and Concrete Research*, vol. 39, n° 8, p. 644‑650, août 2009, doi: 10.1016/j.cemconres.2009.05.012.

[8] S. Blotevogel *et al.*, « Ability of the R3 test to evaluate differences in early age reactivity of 16 industrial ground granulated blast furnace slags (GGBS) », *Cement and Concrete Research*, vol. 130, avr. 2020, doi: 10.1016/j.cemconres.2020.105998.

[9] S. Blotevogel *et al.*, « Effect of TiO_2 and 10 minor elements on the reactivity of ground granulated blast furnace slag (GGBS) in blended cements », *J Am Ceram Soc*, p. jace.17431, sept. 2020, doi: 10.1111/jace.17431.

[10] E. M. J. Berodier, « Impact of the supplementary cementitious materials on the kinetics and microstructural development of cement hydration », EPFL, 2015. doi: 10.5075/epfl-thesis-6417.

[11] V. Kocaba, E. Gallucci, et K. L. Scrivener, « Methods for determination of degree of reaction of slag in blended cement pastes », *Cement and Concrete Research*, vol. 42, n° 3, p. 511‑525, mars 2012, doi: 10.1016/j.cemconres.2011.11.010.

[12] M. Whittaker, M. Zajac, M. Ben Haha, F. Bullerjahn, et L. Black, « The role of the alumina content of slag, plus the presence of additional sulfate on the hydration and microstructure of Portland cement-slag blends », *Cement and Concrete Research*, vol. 66, p. 91‑101, déc. 2014, doi: 10.1016/j.cemconres.2014.07.018.

[13] S. Kucharczyk, J. Deja, et M. Zajac, « Effect of Slag Reactivity Influenced by Alumina Content on Hydration of Composite Cements », *ACT*, vol. 14, n° 9, p. 535‑547, 2016, doi: 10.3151/jact.14.535.

[14] P. T. Durdziński, M. Ben Haha, M. Zajac, et K. L. Scrivener, « Phase assemblage of composite cements », *Cement and Concrete Research*, vol. 99, p. 172‑182, sept. 2017, doi: 10.1016/j.cemconres.2017.05.009.

[15] E. Berodier et K. Scrivener, « Evolution of pore structure in blended systems », *Cement and Concrete Research*, vol. 73, p. 25‑35, juill. 2015, doi: 10.1016/j.cemconres.2015.02.025.

[16] S. Adu-Amankwah, M. Zajac, C. Stabler, B. Lothenbach, et L. Black, « Influence of limestone on the hydration of ternary slag cements », *Cement and Concrete Research*, vol. 100, p. 96‑109, oct. 2017, doi: 10.1016/j.cemconres.2017.05.013.

[17] P. Lawrence, M. Cyr, et E. Ringot, « Mineral admixtures in mortars: Effect of inert materials on short-term hydration », *Cement and Concrete Research*, vol. 33, n° 12, p. 1939‑1947, déc. 2003, doi: 10.1016/S0008-8846(03)00183-2.

[18] W. A. Gutteridge et J. A. Dalziel, « Filler cement: The effect of the secondary component on the hydration of Portland cement », *Cement and Concrete Research*, vol. 20, n° 6, p. 853‑ 861, nov. 1990, doi: 10.1016/0008-8846(90)90046-Z.
[19] E. Gruyaert, N. Robeyst, et N. De Belie, « Study of the hydration of Portland cement blended with blast-furnace slag by calorimetry and thermogravimetry », *J Therm Anal Calorim*, vol. 102, n° 3, p. 941‑ 951, déc. 2010, doi: 10.1007/s10973-010-0841-6.
[20] K. Riding, D. A. Silva, et K. Scrivener, « Early age strength enhancement of blended cement systems by CaCl2 and diethanol-isopropanolamine », *Cement and Concrete Research*, vol. 40, n° 6, p. 935‑ 946, juin 2010, doi: 10.1016/j.cemconres.2010.01.008.
[21] V. S. Ramachandran, « 5 - Accelerators », in *Concrete Admixtures Handbook (Second Edition)*, Park Ridge, NJ: William Andrew Publishing, 1996, p. 185‑ 285. doi: 10.1016/B978-081551373-5.50009-X.
[22] G. Van Rompaey, « Etude de la réactivité des ciments riches en laitier, à basse température et à temps court, sans ajout chloruré », 2006. Consulté le: oct. 05, 2016. [En ligne]. Disponible sur: http://hdl.handle.net/2013/ULB-DIPOT:oai:dipot.ulb.ac.be:2013/210780
[23] V. S. Ramachandran, « Possible states of chloride in the hydration of tricalcium silicate in the presence of calcium chloride », *Mat. Constr.*, vol. 4, n° 1, p. 3‑ 12, janv. 1971, doi: 10.1007/BF02473926.
[24] T. Oey *et al.*, « Comparison of Ca(NO3)2 and CaCl2 Admixtures on Reaction, Setting, and Strength Evolutions in Plain and Blended Cementing Formulations », *J. Mater. Civ. Eng.*, vol. 27, n° 10, p. 04014267, oct. 2015, doi: 10.1061/(ASCE)MT.1943-5533.0001240.
[25] B. E. I. Abdelrazig, D. G. Bonner, D. V. Nowell, J. M. Dransfield, et P. J. Egan, « The solution chemistry and early hydration of ordinary portland cement pastes with and without admixtures », *Thermochimica Acta*, vol. 340‑ 341, p. 417‑ 430, déc. 1999, doi: 10.1016/S0040-6031(99)00286-5.
[26] M. C. G. Juenger, P. J. M. Monteiro, E. M. Gartner, et G. P. Denbeaux, « A soft X-ray microscope investigation into the effects of calcium chloride on tricalcium silicate hydration », *Cement and Concrete Research*, vol. 35, n° 1, p. 19‑ 25, janv. 2005, doi: 10.1016/j.cemconres.2004.05.016.
[27] J. J. Thomas, A. J. Allen, et H. M. Jennings, « Hydration Kinetics and Microstructure Development of Normal and $CaCl_2$ -Accelerated Tricalcium Silicate Pastes », *J. Phys. Chem. C*, vol. 113, n° 46, p. 19836‑ 19844, nov. 2009, doi: 10.1021/jp907078u.
[28] C. Wang, X. Chen, et R. Wang, « Do chlorides qualify as accelerators for the cement of deepwater oil wells at low temperature? », *Construction and Building Materials*, vol. 133, p. 482‑ 494, févr. 2017, doi: 10.1016/j.conbuildmat.2016.12.089.
[29] N. Makaratat, C. Jaturapitakkul, C. Namarak, et V. Sata, « Effects of binder and CaCl2 contents on the strength of calcium carbide residue-fly ash concrete », *Cement and Concrete Composites*, vol. 33, n° 3, p. 436‑ 443, mars 2011, doi: 10.1016/j.cemconcomp.2010.12.004.
[30] B. Pacewska, I. Wilińska, et G. Blonkowski, « Investigations of cement early hydration in the presence of chemically activated fly ash: Use of calorimetry and infrared absorption methods », *J Therm Anal Calorim*, vol. 93, n° 3, p. 769‑ 776, sept. 2008, doi: 10.1007/s10973-008-9143-7.
[31] C. Shi et J. Qian, « Activated blended cement containing high volume coal fly ash », *Advances in Cement Research*, vol. 13, n° 4, p. 157‑ 163, oct. 2001, doi: 10.1680/adcr.2001.13.4.157.
[32] C. Shi et R. L. Day, « Comparison of different methods for enhancing reactivity of pozzolans », *Cement and Concrete Research*, vol. 31, n° 5, p. 813‑ 818, mai 2001, doi: 10.1016/S0008-8846(01)00481-1.
[33] C. Shi et R. L. Day, « Pozzolanic reaction in the presence of chemical activators », *Cement and Concrete Research*, vol. 30, n° 4, p. 607‑ 613, avr. 2000, doi: 10.1016/S0008-8846(00)00214-3.
[34] F. M. Lea, P. C. Hewlett, et M. Liška, *Lea's chemistry of cement and concrete*. 2019.
[35] O. Kayali, M. S. H. Khan, et M. Sharfuddin Ahmed, « The role of hydrotalcite in chloride binding and corrosion protection in concretes with ground granulated blast furnace slag », *Cement and Concrete Composites*, vol. 34, n° 8, p. 936‑ 945, sept. 2012, doi: 10.1016/j.cemconcomp.2012.04.009.

[36] B. Salesses, « Durabilité des matrices ciment Portland - laitier de haut-fourneau activées par des chlorures », Université de Toulouse, Toulouse, 2019.
[37] K. Scrivener, R. Snellings, et B. Lothenbach, *A Practical Guide to Microstructural Analysis of Cementitious Materials*. CRC Press, 2018.
[38] M. Mouret, A. Bascoul, et G. Escadeillas, « Study of the degree of hydration of concrete by means of image analysis and chemically bound water », *Advanced Cement Based Materials*, vol. 6, n° 3, p. 109‑115, oct. 1997, doi: 10.1016/S1065-7355(97)90017-1.
[39] A. C. A. Muller, « Characterization of porosity & C-S-H in cement pastes by ^{1}H NMR », 2014, doi: 10.5075/EPFL-THESIS-6339.
[40] T. Kamada, S. Uchida, et K. Rokugo, « Nondestructive Evaluation of Setting and Hardening of Cement Paste Based on Ultrasonic Propagation Characteristics », *ACT*, vol. 3, n° 3, p. 343‑353, 2005, doi: 10.3151/jact.3.343.
[41] N. Robeyst, E. Gruyaert, C. U. Grosse, et N. De Belie, « Monitoring the setting of concrete containing blast-furnace slag by measuring the ultrasonic p-wave velocity », *Cement and Concrete Research*, vol. 38, n° 10, p. 1169‑1176, oct. 2008, doi: 10.1016/j.cemconres.2008.04.006.
[42] N. De Belie, C. U. Grosse, J. Kurz, et H.-W. Reinhardt, « Ultrasound monitoring of the influence of different accelerating admixtures and cement types for shotcrete on setting and hardening behaviour », *Cement and Concrete Research*, vol. 35, n° 11, p. 2087‑2094, nov. 2005, doi: 10.1016/j.cemconres.2005.03.011.
[43] G. Ye, P. Lura, K. van Breugel, et A. L. A. Fraaij, « Study on the development of the microstructure in cement-based materials by means of numerical simulation and ultrasonic pulse velocity measurement », *Cement and Concrete Composites*, vol. 26, n° 5, p. 491‑497, juill. 2004, doi: 10.1016/S0958-9465(03)00081-7.
[44] N. Shanahan, A. Sedaghat, et A. Zayed, « Effect of cement mineralogy on the effectiveness of chloride-based accelerator », *Cement and Concrete Composites*, vol. 73, p. 226‑234, oct. 2016, doi: 10.1016/j.cemconcomp.2016.07.015.
[45] T. Vehmas, A. Kronlöf, et A. Cwirzen, « Calcium chloride acceleration in ordinary Portland cement », *Magazine of Concrete Research*, vol. 70, n° 16, p. 856‑863, août 2018, doi: 10.1680/jmacr.17.00079.
[46] A. C. Jupe, A. P. Wilkinson, K. Luke, et G. P. Funkhouser, « Slurry Consistency and In Situ Synchrotron X-Ray Diffraction During the Early Hydration of Portland Cements With Calcium Chloride », *J American Ceramic Society*, vol. 90, n° 8, p. 2595‑2602, août 2007, doi: 10.1111/j.1551-2916.2007.01806.x.
[47] U. A. Birnin-Yauri et F. P. Glasser, « Friedel's salt, Ca2Al(OH)6(Cl,OH)·2H2O: its solid solutions and their role in chloride binding », *Cement and Concrete Research*, vol. 28, n° 12, p. 1713‑1723, déc. 1998, doi: 10.1016/S0008-8846(98)00162-8.
[48] W. S. Yum, Y. Jeong, S. Yoon, D. Jeon, Y. Jun, et J. E. Oh, « Effects of CaCl 2 on hydration and properties of lime(CaO)-activated slag/fly ash binder », *Cement and Concrete Composites*, vol. 84, p. 111‑123, nov. 2017, doi: 10.1016/j.cemconcomp.2017.09.001.
[49] Q. Li, Y. Ge, G. Geng, S. Bae, et P. J. M. Monteiro, « $CaCl_2$ -Accelerated Hydration of Tricalcium Silicate: A STXM Study Combined with ^{29} Si MAS NMR », *Journal of Nanomaterials*, vol. 2015, p. 1‑10, 2015, doi: 10.1155/2015/215371.
[50] Y. Elakneswaran, T. Nawa, et K. Kurumisawa, « Zeta potential study of paste blends with slag », *Cement and Concrete Composites*, vol. 31, n° 1, p. 72‑76, janv. 2009, doi: 10.1016/j.cemconcomp.2008.09.007.